Macromolecules **2006,** *39,* 2284−2290

Protein Repellency of Well-Defined, Concentrated Poly(2-hydroxyethyl methacrylate) Brushes by the Size-Exclusion Effect

Chiaki Yoshikawa,[†] Atsushi Goto,[†] Yoshinobu Tsujii,[†] Takeshi Fukuda,*[,†] Tsuyoshi Kimura,[§] Kazuya Yamamoto,[‡] and Akio Kishida[§]

Institute for Chemical Research, Kyoto University, Uji, Kyoto 611-0011, Japan; Department of Nanostructured and Advanced Materials, Graduate School of Science and Engineering, Kagoshima University, 1-21140 Korimoto, Kagoshima 890-0065, Japan; and Institute of Biomaterials and Bioengineering, Tokyo Medical and Dental University, Chiyoda, Tokyo 101-0062, Japan

Received September 17, 2005; Revised Manuscript Received November 10, 2005

ABSTRACT: The adsorption of proteins on poly(2-hydroxyethyl methacrylate) (PHEMA) brushes was systematically studied by quartz crystal microbalance (QCM) and fluorescence microscopy as a function of graft density and protein size. The graft density σ (chains/nm^2) ranged from 0.007 (dilute or semidilute brush regime) to 0.7 (concentrated brush regime), and the protein size ranged from 2 to 13 nm in an effective diameter. The lowest-density brush ($\sigma = 0.007$) adsorbed all the tested four proteins, while the highest-density brush ($\sigma = 0.7$) adsorbed none of them. The middle-density brush ($\sigma = 0.06$) showed an intermediate behavior, adsorbing the smallest two proteins but effectively repelling the largest two. PHEMA cast films adsorbed a probe protein with the adsorbed amount increasing approximately proportionally to the film thickness, indicating that the adsorption mainly occurred in the bulk of the film. The noted results for the brushes support the idea of size-exclusion effect, an effect characteristic of concentrated polymer brushes, in which the graft chains are highly extended and highly oriented so that large molecules, sufficiently large compared with the distance between the nearest-neighbor graft points, are *physically* excluded from the entire brush layer. In this regard, the behavior of the lowest-density brush should be essentially similar to that of the cast film, as was in fact observed.

Introduction

Living radical polymerization (LRP) has been applied to surface-initiated graft polymerization, allowing controlled grafting of well-defined polymers from various solid surfaces with dramatically high surface densities.[1−9] The surface density σ reached as large as 0.7 chains/nm^2 for common polymers like poly(methyl methacrylate) (PMMA) and polystyrene (PS).[9] This density was more than 1 order of magnitude higher than those of typical "semidilute" brushes, going deep into the "concentrated brush" regime which had been little explored systematically because of the unavailability of such brush samples. Recent studies revealed that these concentrated brushes have structure and properties quite different and even unpredictable from those of semidilute brushes:[9] most strikingly, the PMMA concentrated brushes swollen in a good solvent (toluene) exhibited an equilibrium film thickness as large as 80−90% of the full (contour) length of the graft chains, indicating that the chains are extended to a similarly high degree.[9,10] The surface density of 0.7 chains/nm^2 for a PMMA brush, for example, also means that the thickness of the dry film reaches about 40% of the full length of the chains, which is much larger than the mean size of the chains in a random-coil (or so-called "mushroom") conformation. Presumably reflecting this characteristic conformational feature of concentrated brushes, dry PMMA brushes had a glass transition temperature significantly higher,[11] and a plate compressibility markedly smaller,[12] than those of the equivalent cast films. More interestingly, they were immiscible even with free PMMA of an oligomeric chain length.[9,13] This last observation suggests that concentrated brushes in the melt have a size-exclusion effect of (conformational) entropic origin. A similar effect is expectable for concentrated brushes swollen in a good solvent, as, in fact, was demonstrated chromatographically by using the silica monolith column coated with concentrated PMMA brushes.[9,14]

As one of the most interesting potential applications of polymer brushes, attention has been directed toward biointerfaces to tune interactions of solid surfaces with biologically important materials. For example, proteins will adsorb on surfaces through nonspecific interactions, often triggering a biofouling, e.g., the deposition of biological cells, bacteria, and so on. Attempts have been made to modify surfaces with polymer brushes to prevent protein adsorption. To understand the process of protein adsorption, the interactions between proteins and brush-coated surfaces can be modeled by the three generic modes illustrated in Scheme 1a (after Curie et al.[15] with some modifications). One is the primary adsorption, in which a protein diffuses into the brush and adsorbs on the substrate surface. The secondary adsorption is the one occurring at the outermost surface of the swollen brush film. The last one is the tertiary adsorption, which is caused by the interaction of protein with the polymer segments within the brush layer. For relatively small proteins, the primary and tertiary adsorptions would be particularly important, but they should become less important with increasing protein size and increasing graft density, since a larger protein would be more difficult to diffuse against the concentration gradient formed by the polymer brush, and this gradient, clearly, is a function of graft density. However, the size and density dependence of protein adsorption would manifest itself much more clearly for concentrated brushes due to a different mechanism. As already noted, the graft chains in

[†] Kyoto University.
[‡] Kagoshima University.
[§] Tokyo Medical and Dental University.
* Corresponding author: e-mail fukuda@scl.kyoto-u.ac.jp.

10.1021/ma0520242 CCC: $33.50
Published on Web 02/25/2006

Scheme 1. Schematic Illustration of (a) Possible Interactions of Probe Molecules with a Polymer Brush and (b) Size-Exclusion Effect of Concentrated Brush

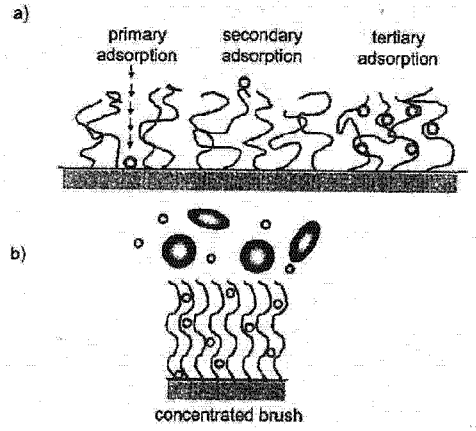

a concentrated brush are highly extended and hence highly oriented so that the entire brush layer, from the substrate surface to the outermost surface throughout, could have a size-exclusion effect (Scheme 1b). By the terms "size exclusion", we stress the *physical* aspect of the phenomenon, meaning that the protein (or probe molecule) is excluded from the brush layer to avoid the large (mainly conformational) entropy loss caused on the highly extended chains by the entrance of the large molecule. Since the degree of chain extension is much less significant in semidilute brushes, this effect should be minor for them.

In the past, poly(ethylene oxide) (PEO)-grafted surfaces were extensively studied to discuss their protein adsorption behavior as a function of graft density.[15−21] However, since those surfaces were prepared by physisorption of block copolymers or comb-like polymers using a self-assembling or the Langmuir−Blodgett technique, the graft density should have been in a semidilute regime, i.e., too low to observe the mentioned effect clearly, if any present. Well-defined concentrated brushes achievable by surface-initiated LRP would set up size-exclusion limits at much smaller sizes of probe molecules, thus allowing us to explore them with available proteins. Most recently, poly(acrylamide),[22] poly(2-(dimethylamino)ethyl methacrylate),[23] poly(oligo(ethylene glycol) methyl methacrylate),[24] and poly(2-methacryloxyethylphosphorylcholine) (PMPC)[25−27] brushes were prepared by surface-initiated LRP and observed to show good adsorption resistance for proteins and cells. From a mechanistic point of view, however, these studies remained purely qualitative, paying little attention to the mentioned characteristics of concentrated brushes.

In this work, we have attempted to substantiate the postulated size-exclusion effect of concentrated polymer brushes by systematically studying the adsorption behavior of varying sizes of proteins on the substrates grafted with a poly(2-hydroxyethyl methacrylate) (PHEMA) brush of varying surface densities, by means of quartz crystal microbalance (QCM) and fluorescence microscopy. PHEMA is a hydrophilic, biocompatible polymer,[28] but the biocompatibility of PHEMA cast film is reported to be not as good as e.g. PMPC[29,30] and poly(2-methoxyethyl acrylate) cast films.[31,32] Hence, any favorable results that PHEMA brushes may present could be ascribed more to the structural, rather than thermodynamic, properties of the system. Our ultimate goal is to develop, by utilizing the advantages of surface-initiated LRP,[9] a concentrated brush-based, new biointerface that will completely suppress the adsorption of small as well as large proteins. This work should be an important step for this goal.

Scheme 2. Schematic Illustration of Graft Polymerizations on an Inorganic Substrate: (a) Surface-Initiated ATRP and (b) a Grafting-To Method

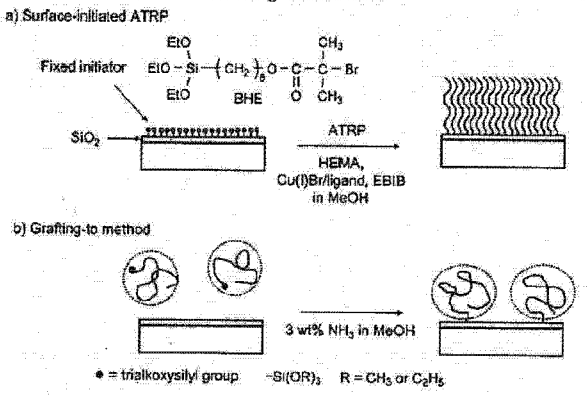

Experimental Section

Materials. 2-Hydroxyethyl methacrylate (HEMA) (99%, Nacalai Tesque, Japan) was purified according to the literature.[33] Cu(I)Br (99.9%, Wako Pure Chemical, Japan), ethyl 2-bromoisobutylate (EBIB) (99%, Wako), 2,2-bipyridine (bpy) (99%, Nacalai), methanol (99%, Nacalai), phosphate-buffered saline (PBS) (pH = 7.4, Wako), ammonia (28% aqueous, Nacalai), 3-mercaptopropyltrimethoxysilane (S810) (Chisso, Japan), and 2,2′-azobis(4-methoxy-2,4-dimethylvaleronitrile) (V70) (99.9%, Wako) were used as received. 6-(2-Bromo-2-isobutyloxy)hexyltriethoxysilane (BHE), a fixable initiator for ATRP, was prepared, as previously reported.[34] Bovine serum aprotinin (Aprotinin), bovine serum albumin (BSA), fluorescein isothiocyanate-labeled BSA (FITC-BSA), bovine serum immunoglobulin G (IgG), and horse heart myoglobin (Myoglobin) were purchased from Sigma-Aldrich and used as received.

Silicon wafers were cleaned by ultrasonication in $CHCl_3$ for 30 min and ultraviolet (UV)/ozone treatment for 10 min. The UV/ozone treatment effectively removed organic contaminants on the wafer surfaces. QCM chips (optically polished square-shaped AT-cut quartz crystals (1 × 1 cm^2) with gold electrodes) (Seiko EG&G, Seiko Instruments Inc.) were similarly cleaned. On the cleaned chip, Cr and then SiO_2 were deposited in a vacuum with the thicknesses of 5 and 40 nm, respectively.

Preparation of High-Density Brushes (σ = 0.7 Chains/nm^2). High-density PHEMA brushes were prepared by surface-initiated ATRP, as shown in Scheme 2a. A silicon wafer and a SiO_2-deposited QCM chip were immersed in a tetrahydrofuran (THF) solution of BHE (1 wt %) and NH_3 (1 wt %) for 12 h at room temperature and washed with THF. The BHE-immobilized substrate (wafer and chip) was immersed in a degassed methanol solution of HEMA (4.5 M), Cu(I)Br (25 mM), bpy (63 mM), and the free initiator EBIB (22.5 mM), sealed under vacuum in a glass tube (1 cm diameter), and heated at 40 °C for a prescribed time. This polymerization condition was referred to Armes et al., who successfully prepared low-polydispersity free polymers of HEMA.[35] After polymerization, the solution was diluted with *N*,*N*-dimethylformamide (DMF) to a known concentration and analyzed by gel permeation chromatography (GPC). The conversion was determined from the GPC peak area. The substrate was rinsed in a Soxhlet apparatus with methanol for 5 h to remove physisorbed free polymers and impurities.

Preparation of Middle- and Low-Density Brushes (σ = 0.06 and 0.007 Chains/nm^2). Middle- and low-density PHEMA brushes were prepared by a grafting-to method, as shown in Scheme 2b. Namely, PHEMA chains with an alkoxysilyl group at one chain end were immobilized on a silicon wafer and a SiO_2-deposited QCM chip in solution. Two end-functionalized PHEMAs with different chain lengths were used. The shorter one (M_n = 9800 and M_w/M_n = 1.2) was synthesized by ATRP with BHE (with a triethoxysilyl group) used as a free initiator: a degassed methanol solution of HEMA (4.5 M), BHE (22.5 mM), Cu(I)Br (25 mM), and bpy (63

Table 1. Characteristics of Studied PHEMA Surfaces

surface[a]	$M_{n,conv}$[b]	$M_{n,PEG}$[c]	M_w/M_n[c]	L[d]/(nm)	σ[e]/(chain nm^{-2})	d[f]/(nm)	θ[g]/(deg)
high-density brush	1700	3500	1.21	2	0.7	1	29
high-density brush	9700	8000	1.26	10	0.7	1	
high-density brush	16800[h]	12300	1.30	15	0.7	1	29
middle-density brush	19000	15300	1.27	2	0.06	4	27
low-density brush		1.2×10^5	1.24	2	0.007[i]	12	29
cast film		$>4 \times 10^5$		30			23
cast film		$>4 \times 10^5$		90			23
cast film		$>4 \times 10^5$		330			23
BHE[j]							55

[a] Characteristics of brushes were almost identical on silicon wafers and QCM chips, and typical values on silicon wafers are listed. [b] Calculated according to eq 3. [c] Estimated by PEG-calibrated GPC. [d] Film thickness, the error is within 10%. [e] Graft density, calculated with L and $M_{n,conv}$ according to eq 2. [f] Average distance between the nearest-neighbor graft points, calculated according to $d = \sigma^{-1/2}$. [g] Contact angle; the error is within 2°. [h] The $M_{n,MALLS}$ is 17600 (see text). [i] Calculated with L and $M_{n,MALLS}$ (1.8×10^5) according to eq 2. [j] BHE-immobilized surface.

mM) was heated at 30 °C for 1 h. After reprecipitation with cooled water, there was isolated a PHEMA ($M_n = 1.5 \times 10^4$ and $M_w/M_n = 1.2$) possessing a triethoxysilyl group (derived from BHE) at one chain end. A silicon wafer and a SiO_2-deposited QCM chip were immersed in a methanol solution of the PHEMA (1 wt %) and NH_3 (2 wt %) for 12 h at room temperature and rinsed in a Soxhlet apparatus with methanol for 5 h, yielding a middle-density brush ($\sigma = 0.06$ chains/nm^2).

The longer end-functionalized PHEMA was prepared by the conventional radical polymerization with the chain transfer agent S810: a methanol solution of HEMA (4.5 M), S810 (chain transfer agent; 9 mM), and V70 (9 mM) was heated at 40 °C for 2 h. The obtained polymer was fractionated by use of a preparative GPC, yielding a PHEMA ($M_n = 1.2 \times 10^5$ and $M_w/M_n = 1.2$) possessing a trimethoxysilyl group (derived from S810) at one chain end. This polymer was immobilized on a silicon wafer and a SiO_2-deposited QCM chip as described above, yielding a low-density brush ($\sigma = 0.007$ chains/nm^2).

Preparation of Cast Films. PHEMA ($M_v = 10^6$) (Aldrich), after having purified by reprecipitation from a methalol solution into cold water, was dissolved in methanol. The cast films were obtained by spin-casting the PHEMA solution onto a silicon wafer using a homemade spin-coater at a spinning speed of 2000 rpm for 2 min, followed by annealing at 80 °C for 24 h in a vacuum. The film thickness was controlled by changing the concentration of PHEMA solution.

QCM Measurement. Protein adsorption was studied at 25 °C with a quartz crystal analyzer 917 (Seiko EG&G) driving a 9 MHz QCM chip. The QCM chip was mounted in a thermostated homemade QCM cell by means of O-ring seals, which allowed only one face of the chip to come in contact with the solution. Before injection of a PBS solution of a protein, the QCM cell was initially filled with PBS and rinsed several times until a stable baseline was established. The stability of the frequency of QCM was ±0.3 Hz within 1 h at 25 °C in water. The adsorbed amount Δm (ng) is represented by[36]

$$\Delta m = -\Delta f A((\mu_q \rho_q)/(2F_q^2))^{1/2} \quad (1)$$

where Δf is the frequency change (Hz), F_q is the parent frequency of QCM (9 MHz), μ_q is the shear modules of quartz (2.947×10^{11} g/(cm s^2)), ρ_q is the density of quartz (2.648 g/cm^3), and A is the surface area of electrode (0.196 cm^2).

Fluorescence Microscopic Observation. The sample was immersed in a PBS solution of FITC-BSA (1.0 g/L) for a prescribed time at room temperature. The sample was washed by softly immersing in PBS, and this procedure was repeated five times with fresh PBS. Fluorescence images were taken on an optical microscope (Eclipse TE2000, Nikon, Tokyo, Japan) equipped with a highly sensitive CCD camera (ORCA-ER, Hamamatsu Photonics, Shizuoka, Japan). The observation was made on at least five spots for each sample, and the fluorescence intensities of these spots were averaged. To check reproducibility of the FITC-BSA adsorption, at least three samples were prepared under the same conditions and examined.

Other Measurements. The GPC analysis for PHEMA was made on a Tosoh CCP&8020 series high-speed liquid chromatograph (Tokyo, Japan) equipped with two Shodex gel columns LF804 (300 × 80 mm; bead size = 6 μm; pore size = 20−3000 Å) (Tokyo). DMF was used as eluent with a flow rate of 0.8 mL/min (40 °C). The column system was calibrated with Tosoh standard poly(ethylene glycol)s (PEGs). Sample detection and quantification were made with a Tosoh differential refractometer RI-8020. Sample detection was also made with a multiangle laser light scattering (MALLS) detector, a Wyatt Technology DAWN EOS (Santa Barbara, CA), equipped with a Ga−As laser ($\lambda = 690$ nm). The refractive index increment dn/dc was determined to be 0.075 mL g^{-1} by a Wyatt Technology OPTILAB DSP differential refractometer ($\lambda = 690$ nm).

For the GPC analysis of proteins, the above-noted chromatograph equipped with a Shodex gel column KW804 (300 × 80 mm; bead size = 7 μm; pore size = 300 Å) (Tokyo) was calibrated with Shodex standard pullulans. PBS was used as eluent with a flow rate of 0.8 mL/min (30 °C).

The fractionation of PHEMA was made on a preparative LC-918 liquid chromatograph (Japan Analytical Industry, Tokyo) equipped with JAIGEL GS-510 poly(vinyl alcohol) gel columns (500 × 21.5 mm; bead size = 16 μm). Methanol was used as eluent with a flow rate of 5.0 mL/min (room temperature).

The thicknesses of the deposited Cr and SiO_2 and the grafted and spin-casted PHEMA layers were determined by a compensator-rotating, spectroscopic ellipsometer (M-2000U, J.A. Woolam, Lincoln, NE) equipped with D_2 and QTH lamps. The polarizer angle was 45°, and the incident angles were 60°, 65°, and 70°. From the ellipsometric data, the thickness of PHEMA layer was evaluated using the optical constants determined for the spin-cast layer with a thickness of ca. 200 nm. The graft density σ was estimated from

$$\sigma = L\rho N_A/M_n \quad (2)$$

where L is the thickness of graft layer, ρ is the bulk density of PHEMA (1.15 g/cm^3), N_A is the Avogadro number, and M_n is the number-average molecular weight.

Contact angles (θ) were measured at room temperature with a contact angle meter CA-X (Kyowa Interface Science, Saitama, Japan). The measurement was made on at least five spots for each sample, and these θ values were averaged.

Results and Discussion

Preparation and Characterization of PHEMA Brushes. The "high-density" PHEMA brushes were prepared by surface-initiated ATRP. A few previous reports dealt with surface-initiated LRP of HEMA,[37−39] but we made an independent effort to optimize polymerization conditions to meet our purpose. Three samples with different chain lengths of PHEMA (and hence, different thicknesses of the graft layer) were prepared by varying the polymerization time. Table 1 lists the M_n and M_w/M_n of the free polymers simultaneously produced from the free initiator in the solution. These values can be used as

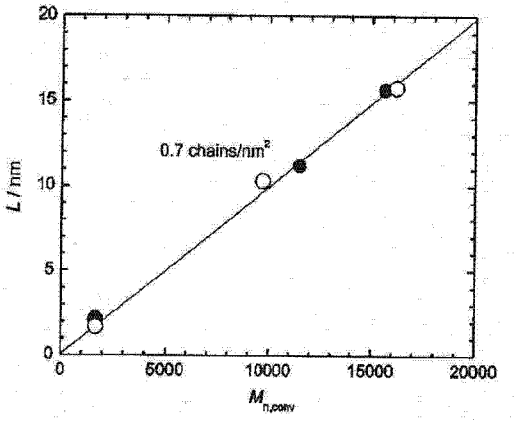

Figure 1. Plot of L vs $M_{n,conv}$ for the high-density brushes prepared on (●) silicon wafer and (○) QCM chip.

sufficiently accurate indices for those of the graft polymers.[4] The M_w/M_n was 1.2−1.3 in all cases, suggesting a well-controlled polymerization. The $M_{n,conv}$ was calculated using the following equation:

$$M_{n,conv} = [HEMA]_0/[EBIB]_0 \times MW \times C/100 \quad (3)$$

where $[HEMA]_0$ and $[EBIB]_0$ are the feed concentration of HEMA and EBIB, respectively, MW is the molecular weight of HEMA, and C is the monomer conversion in percent. This value is the theoretical M_n for an ideal living polymerization. To evaluate the absolute value of M_n, the GPC detection was made with a MALLS detector for the highest-molecular-weight sample (prepared by the ATRP): the thus-determined M_n ($M_{n,MALLS}$ = 17 600) agreed well with the theoretical value ($M_{n,conv}$ = 16 800) rather than the PEG-calibrated M_n ($M_{n,PEG}$ = 12 300). For the oligomeric PHEMAs prepared by nearly the same ATRP system, Ames et al. reported that the absolute M_n determined by NMR was approximately equal to the $M_{n,conv}$.[35] We will use $M_{n,conv}$ for the absolute value.

The thickness L of the graft layer measured by ellipsometry linearly increased with increasing $M_{n,conv}$ of the free polymer (see Figure 1), suggesting a uniform growth of graft polymer with a constant surface density. From the slope of the line in Figure 1, the graft density σ was estimated to be ca. 0.7 chains/nm², which is similar to the highest values reported for PMMA and PS brushes.[9] Brushes with lower graft densities were prepared by a grafting-to method using two end-functionalized PHEMAs with $M_n = 1.5 \times 10^4$ and 1.2×10^5. They gave the "middle-density" (σ = 0.06 chains/nm²) and "low-density" (σ = 0.007 chains/nm²) brushes, respectively. These PHEMA brushes can be grouped into two series: one series is the high-density brushes with a nearly constant graft density of 0.7 chains/nm² and different dry film thicknesses 2, 10, and 15 nm, and the other is the brushes with nearly the same dry film thickness of 2 nm and different graft densities 0.007, 0.06, and 0.7 chains/nm².

The contact angle θ was measured in water by the air-bubble method for these brushes as well as a BHE-immobilized wafer and three PHEMA spin-cast films of thicknesses 30, 90, and 330 nm (Table 1). The BHE-immobilized surface (nongrafted surface) was much more hydrophobic than the PHEMA-coated samples (brushes and cast films). The brushes had a θ value slightly (about 5°) higher than the cast films (the experimental error in θ was ±2°), for an unclear reason. The observed dependence (or independence) of θ on graft density and film thickness suggests that the substrate was completely covered

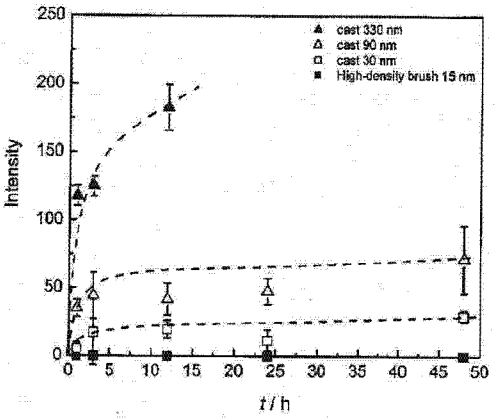

Figure 2. Plot of fluorescence intensity of adsorbed FITC-BSA vs soaked time t (25 °C) for the cast films with L = (▲) 330 nm, (△) 90 nm, and (□) 30 nm and the high-density brush with L = 15 nm (■). The FITC-BSA concentration was 1.0 g/L.

with PHEMA segments in all cases. The effect of the chain end (bromine for the high- and middle-density brushes and hydrogen for the low-density brush) is not evident even for the high-density brushes, in which, because of their oriented structure stressed above, the free chain ends and hence the bromine groups should be populated in the outermost surface of the film.

Adsorption of BSA. By fluorescence microscopy, we examined the adsorption of BSA on PHEMA cast film as a function of thickness: the cast films with different thicknesses (L = 30, 90, and 330 nm) prepared on silicon wafers were soaked in a FITC-BSA solution (1 g/L) at room temperature for a prescribed time, rinsed with PBS, and then observed by a fluorescence microscope. The fluorescence intensity was almost unchanged by further rinsing with PBS, confirming an irreversible adsorption. The fluorescence images suggested that BSA was homogeneously adsorbed (in an optical microscopic scale). Figure 2 shows the plot of fluorescence intensity vs soaked time. Unfortunately, the fluorescence intensity was not calibrated to the amount of adsorbed BSA, but the proportional relationship between them may reasonably be assumed. As a rough measure of the adsorbed amount, we may refer to the previous study reporting that 0.38 μg/cm² of BSA was adsorbed on PHEMA cast films.[32] The fluorescence intensity and hence the amount of adsorbed BSA gradually increased in several hours, approaching a constant (saturation) value. As Figure 3 shows, the intensity at 12 h, as a measure of the saturation value, increased almost proportionally to film thickness L. This means that BSA diffuses deeply into the bulk of the cast film, and that the adsorption in this system consists mainly of the tertiary adsorption with minor contributions of the primary and secondary ones. It naturally took a very long time to reach the saturation value (as compared with the case of high-density brush samples, for example, to be described below).

Next, we examined the adsorption of BSA on the brushes and the BHE-immobilized surfaces by QCM. This method allows in situ monitoring of the adsorption process with a usually high sensitivity. However, when it is applied to a viscoelastic layer in solution, the dissipation effect causes an error in estimating the mass according to eq 1. This error becomes larger with increasing layer thickness, and for this reason, our cast films were too thick to apply QCM. We confirmed that the QCMs with different fundamental frequencies (5 and 9 MHz) gave a consistent result for the brush samples with L = 10 nm or thinner, meaning that the dissipation effect was minor for

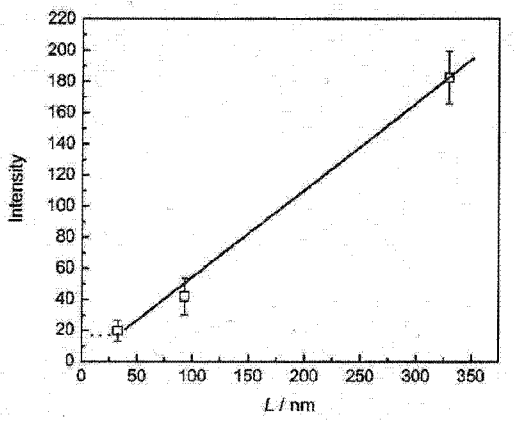

Figure 3. Plot of intensity of adsorbed FITC-BSA vs L for the cast films soaked for 12 h (25 °C). The FITC-BSA concentration was 1.0 g/L.

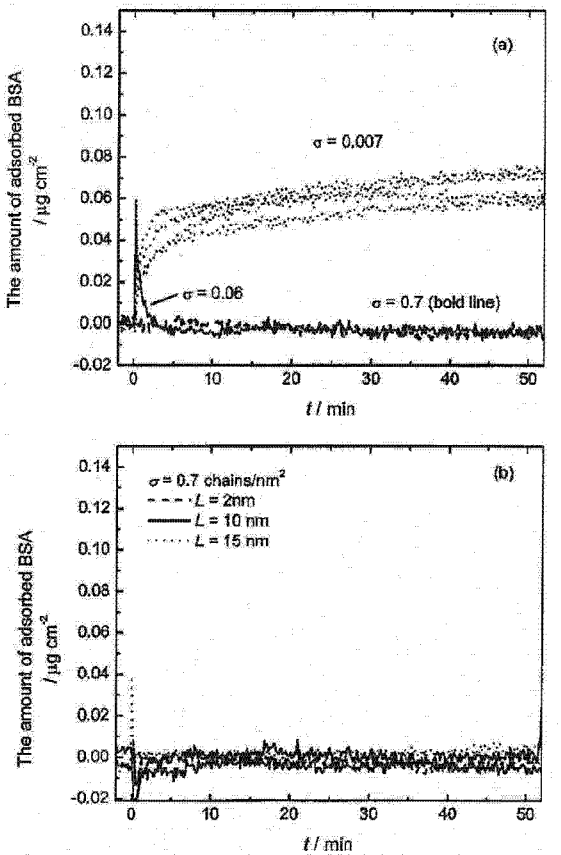

Figure 4. Time evolution of the amount of adsorbed BSA (25 °C) on (a) PHEMA brushes (σ = 0.007, 0.06, and 0.7 chains/nm^2) with L = 2 nm and (b) high-density PHEMA brushes (σ = 0.7 chains/nm^2) with L = 2, 10, and 15 nm. The BSA concentration was 1.0 g/L.

them. Figure 4 shows the results of the QCM measurement (25 °C) at an early stage of adsorption (<1 h), where the concentration of BSA in solution was 1 g/L. The adsorbed amount of BSA given in the ordinate axis was calculated from the frequency change according to eq 1. A sharp peak appearing, in some cases, immediately after the injection of BSA is due to the slight change in pressure and/or temperature on injection. The amount of BSA adsorbed onto the BHE-immobilized surface was 0.28 μg/cm^2 at 1 h (the data not shown), which is close to the value (0.25 μg/cm^2) reported for the side-on monolayer adsorption of BSA.[40] To confirm reproducibility of the measurement, we conducted at least five runs for each sample (an example is given for the low-density brush in Figure 4a, suggesting an experimental error of ±10%). BSA was readily (within 10 min) adsorbed on the low-density brush as well as the BHE surface and not desorbed by washing with PBS, indicating an irreversible adsorption. The amount of BSA adsorbed on the low-density brush at 1 h was ca. 0.07 μg/cm^2 (see Figure 4a), which is smaller than that for the BHE surface but still significant. On the other hand, there was no detectable adsorption on the middle- and high-density brushes (Figure 4a) with L = 2 nm. Figure 4b also shows that the high-density brushes with different thicknesses (L = 2, 10, and 15 nm) were all free from adsorption. These data clearly demonstrate that, by increasing the graft density, the adsorption of BSA can be suppressed. BSA has an ellipsoidal shape with an approximate dimension of 3 × 8 × 9 nm^3,[40–43] while the average distance d (= $\sigma^{-1/2}$) between the nearest-neighbor graft points is approximately 12, 4, and 1 nm for σ = 0.007, 0.06, and 0.7 chains/nm^2, respectively (Table 1). This reasonably suggests that BSA is difficult to diffuse into the swollen layer of the middle- and high-density brushes, on which no adsorption of BSA was, in fact, observed. The longer-term stability of protein repellency on the high-density brushes was studied by fluorescence microscopy, for the QCM experiment was difficult due to a baseline drift: no adsorption of FITC-BSA was detected on them even after 2 days.

Table 2. Absolute and Pullulan-Calibrated Molecular Weights, Crystallographic Dimensions, and $2R_g$ for Studied Proteins

protein	mol wt M	pullulan-calibrated M	crystallographic dimensions/nm	$2R_g$[a]/nm
Aprotinin	6 500	1 500		2
Myoglobin	17 000	5 900	3 × 4 × 4	4
BSA	67 000	22 800	3 × 8 × 9	10
IgG	146 000	35 000		13

[a] Calculated (see text).

Adsorption of Proteins with Different Sizes. QCM experiments were conducted with the brush samples for a series of proteins with different sizes: Aprotinin (molecular weight = 6500), Myoglobin (17 000), BSA (67 000), and IgG (146 000). The characteristics of the four proteins are listed in Table 2. As the size of protein, crystallographic data are available for Myoglobin and BSA but not for the other two. The apparent molecular weights of these four proteins estimated by pullulan-calibrated GPC were 1500, 5900, 23 000, and 35 000 for Aprotinin, Myoglobin, BSA, and IgG, respectively, from which their radii of gyration (R_g) were estimated to be 1, 2, 5, and 6.5 nm, respectively, by using the known relation[44,45] between the R_g and molecular weight of pullulan. As shown in Table 2, the values of $2R_g$ may be good indices for the protein size (compare these values with the crystallographically determined dimensions of Myoglobin and BSA).

Figure 5 shows the amount of adsorbed protein after 1 h of soaking. The low-density brush adsorbed all the proteins, the middle-density one adsorbed only Aprotinin and Myoglobin, and the high-density one adsorbed none. These data show a clear dependence of adsorption on protein size and brush density: very crudely, we can state that no significant adsorption of protein takes place on a PHEMA brush when the brush d is smaller than the protein $2R_g$.

All these results confirm the size-exclusion effect of concentrated brushes. This effect would reduce the primary and tertiary adsorptions but not necessarily the secondary adsorption.

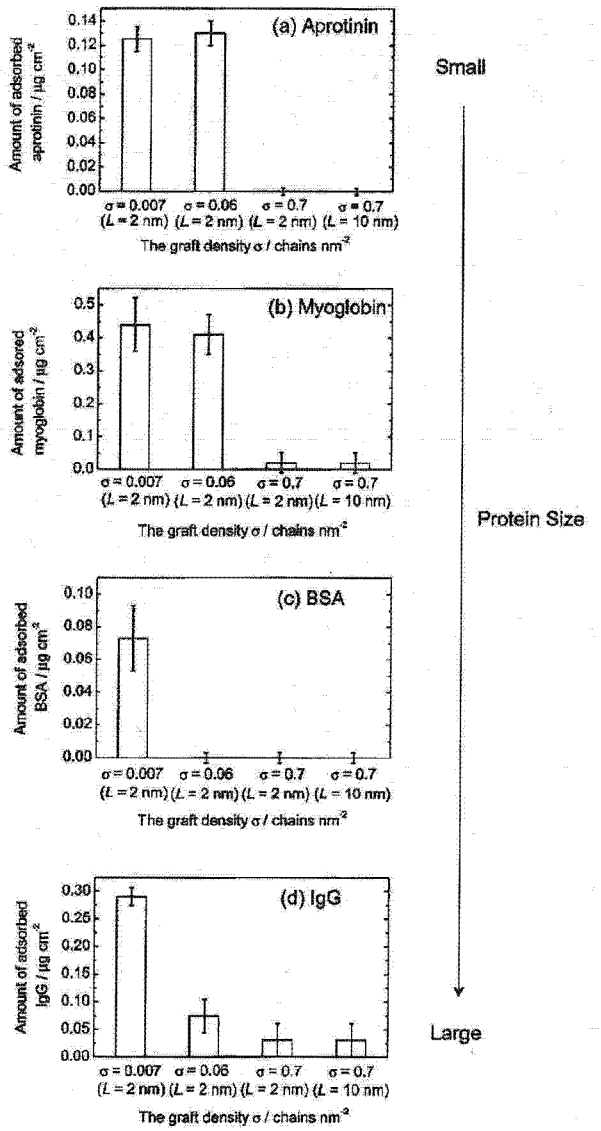

Figure 5. Amounts of adsorbed proteins onto PHEMA brush surfaces, soaked for 1 h (25 °C): (a) Aprotinin, (b) Myoglobin, (c) BSA, and (d) IgG. The protein concentration was 1.0 g/L in all cases.

The secondary adsorption can be induced by two possible interactions: one is the van der Waals and/or Coulombic interaction between the protein and the substrate, which should depend on the thickness of the brush layer.[15] The other is the interaction between the protein and the brush itself (at its outermost surface). The latter possibly depends on e.g. the water content of the brush layer,[46] the mobility of the brush chain,[47] and the structure of water near the brush surface.[31,32] Even though these details remain to be explored, the fact that no significant adsorption of any protein was detected on the high-density PHEMA brush indicates that the secondary adsorption is unimportant for this brush and these proteins. Figure 5 may indicate a nonnegligible adsorption of IgG on the high-density brush, but this may be ascribed to the insufficient number of trials, since another type of independent test (not shown here), which consisted of cycles of protein injection and rinsing, gave no indication of adsorption of this and other proteins on the high-density brush. To be stressed is the above-noted fact that the high-density brushes of different thickness repelled a protein (BSA) equally effectively. This means, on one hand, that no thick brush is needed for this purpose and, on the other hand, that a thick brush has a size-exclusion effect from its bottom to the outer surfaces through out. This is the very feature expected for a concentrated brush.

Finally, a comment is due regarding the block copolymer of PHEMA-PS type. Even though PHEMA cast films themselves have rather poor biocompatibility, as we have observed for the protein repellency, PHEMA-PS block copolymers are known to show improved biocompatibility.[48,49] At first, this improved biocompatibility was considered to have something to do with a microdomain surface structure caused by the phase separation of the PHEMA and PS segments. However, the ground for this interpretation seemed to have been lost, when the later structural studies on the cast films of these block copolymers revealed that the outermost surface of the films in water was preferentially covered with the laterally phase-separated PHEMA layer.[50−52] On the basis of our results, we would suggest the formulation of a concentrated brushlike structure of the PHEMA layer, in which the PHEMA chains are extruding out into the water phase from the hydrophobic (unswollen) PS layer, thereby repelling proteins or other large molecules by a size-exclusion effect.

Conclusions

The cast films and low-density brush ($\sigma = 0.007$ chains/nm^2) of PHEMA showed poor resistance against protein adsorption, which was reasonably ascribed to the tertiary adsorption, i.e., the adsorption induced by the interaction within the bulk of the PHEMA layer. On the other hand, the high-density brush ($\sigma = 0.7$ chains/nm^2) showed excellent resistance even for a protein as small as Aprotinin, independently of the brush thickness ($L = 2-15$ nm). The middle-density brush showed an intermediate behavior, adsorbing smaller proteins but effectively repelling larger proteins. There was a good correlation between the protein size and the threshold graft density beyond which the protein does not adsorb. (The secondary adsorption, occurring on the outermost surface of the PHEMA brushes, was inherently weak for the studied proteins.) These results confirmed the idea of size-exclusion effect of concentrated brushes. In general, it is suggested that the surface adsorption of large molecules like proteins can be greatly suppressed by densely grafting a polymer, i.e., controlling the *physical structure* of the polymer layer. With other unique properties of concentrated polymer brushes along with a range of possibility to design chain architecture by LRP, PHEMA concentrated brushes will find a wide variety of applications as a novel biointerface, such as biochips, biosensors, bioseparators, and medical body implants.

Acknowledgment. We thank Japan Analytical Industry (Tokyo) for the fractionation of PHEMA by preparative GPC. This work was supported by Grant-in-Aids for Scientific Research, the Ministry of Education, Culture, Sports, Science and Technology, Japan (Grant-in-Aids 17002007 and 17205022).

References and Notes

(1) Ejaz, M.; Yamamoto, S.; Ohno, K.; Tsujii, Y.; Fukuda, T. *Macromolecules* **1998**, *31*, 5934.
(2) Huang, X.; Wirth, M. J. *Macromolecules* **1999**, *32*, 1694.
(3) Matyjaszewski, K.; Miller, P. J.; Shukla, N.; Immaraporn, B.; Gelman, A.; Luokala, B. B.; Siclovan, T. M.; Kickelbick, G.; Vallant, T.; Hoffmann, H.; Pakula, T. *Macromolecules* **1999**, *32*, 8716.
(4) Husseman, M.; Malmstrom, E. E.; McNamara, M.; Mate, M.; Mecerreyes, D.; Benoit, D. G.; Hedrick, J. L.; Mansky, P.; Huang, E.; Russell, T. P.; Hawker, C. J. *Macromolecules* **1999**, *32*, 1424.
(5) Kim, J.-B.; Bruening, M. L.; Baker, G. L. *J. Am. Chem. Soc.* **2000**, *122*, 7616.
(6) Zhao, B.; Brittain, W. J. *Prog. Polym. Sci.* **2000**, *25*, 677.

(7) Pyun, J.; Kowalewski, Y.; Matyjaszewski, K. *Macromol. Rapid Commun.* **2003**, *24*, 1043.
(8) Edmonsdon, S.; Osborne, V. L.; Huck, W. T. S. *Chem. Soc. Rev.* **2004**, *33*, 14.
(9) Tsujii, Y.; Ohno, K.; Yamamoto, S.; Goto, A.; Fukuda, T. *Adv. Polym. Sci.*, in press.
(10) (a) Yamamoto, S.; Ejaz, M.; Tsujii, Y.; Matsumoto, M.; Fukuda, T. *Macromolecules* **2000**, *33*, 5602. (b) Yamamoto, S.; Ejaz, M.; Tsujii, Y.; Fukuda, T. *Macromolecules* **2000**, *33*, 5608.
(11) Yamamoto, S.; Tsujii, Y.; Fukuda, T. *Macromolecules* **2002**, *35*, 6077.
(12) Urayama, K.; Yamamoto, S.; Tsujii, Y.; Fukuda, T.; Neher, D. *Macromolecules* **2000**, *35*, 9459.
(13) Yamamoto, S.; Tsujii, Y.; Fukuda, T.; Torikai, N.; Takeda, M. *KENS Rep.* **2001−2002**, *14*, 204.
(14) He, H.; Tsujii, Y.; Fukuda, T.; Nakanishi, K.; Ishizuka, N.; Minakuchi, H. *Polym. Prepr., Jpn. (Soc. Polym. Sci., Jpn.)* **2003**, *52*, 2961.
(15) Currie, E. P. K.; Norde, W.; Cohen Stuart, M. A. *Adv. Colloid Interface Sci.* **2003**, *100−102*, 205.
(16) (a) Jeon, S. I.; Lee, J. H.; Andrade, J. D.; Degennes, P. G. *J. Colloid Interface Sci.* **1991**, *142*, 149. (b) Jeon, S. I.; Andrade, J. D. *J. Colloid Interface Sci.* **1991**, *142*, 159.
(17) Halperin, A. *Langmuir* **1999**, *15*, 2525.
(18) Unsworth, L. D.; Sheardown, H.; Brash, J. L. *Langmuir* **2005**, *21*, 1036.
(19) Norde, W.; Gage, D. *Langmuir* **2004**, *20*, 4162.
(20) Kenausis, G. L.; Voros, J.; Elbert, D. L.; Huang, N.; Hofer, R.; Ruiz-Taylor, L.; Textor, M.; Hubbel, J. A.; Spencer, N. D. *J. Phys. Chem. B* **2000**, *104*, 3298.
(21) Efremove, N. V.; Boundurant, B.; O'Brien, D. F.; Leckband, D. E. *Biochemistry* **2000**, *39*, 3441.
(22) Xiano, D.; Zhang, H.; Wirth, M. *Langmuir* **2002**, *18*, 9971.
(23) Lee, S. B.; Koepsel, R. R.; Morley, S. W.; Matyjaszewski, K.; Sun, Y.; Russell, A. J. *Biomacromolecules* **2004**, *5*, 877.
(24) Ma, H.; Hyun, J.; Stiller, P.; Chikoti, *A. Adv. Mater.* **2004**, *16*, 338.
(25) Feng, W.; Brash, J. L.; Zhu, S. *J. Polym. Sci., Part A: Polym. Chem.* **2004**, *42*, 2931.
(26) Iwata, R.; Suk-In, P.; Hoven, V. P.; Takahara, A.; Akiyoshi, K.; Iwasaki, Y. *Biomacromolecules* **2004**, *5*, 2308.
(27) Feng, W.; Zhu, S.; Ishihara, K.; Brash, J. L. *Langumuir*, in press.
(28) Montheard, J. P.; Chatzopoulos, M.; Chappard, D. *J. Macromol. Sci., Rev. Macromol. Chem. Phys.* **1992**, *C32*, 1.
(29) (a) Ishihara, K.; Aragaki, R.; Ueda, T.; Watanabe, A.; Nakabayashi, N. *J. Biomed. Mater. Res.* **1990**, *24*, 1069. (b) Ishihara, K.; Ziats, N. P.; Tierney, B. P.; Nakabayashi, N.; Anderson, J. M. *J. Biomed. Mater. Res.* **1991**, *25*, 1397.
(30) Sawada, S.; Sakaki, S.; Iwasaki, Y.; Nakabayashi, N.; Ishihara, K. *J. Biomed. Mater. Res.* **2003**, *3*, 411.
(31) Tanaka, M.; Motomura, T.; Kawada, M.; Anzai, T.; Kasori, Y.; Shiroya, T.; Shimura, K.; Onishi, M.; Mochizuki, A. *Biomaterials* **2000**, *21*, 1471.
(32) Tanaka, M.; Mochizuki, A.; Motomura, T.; Shimura, K.; Onishi, M.; Okahata, Y. *Colloids Surf., A* **2001**, *193*, 145.
(33) Beers, L. K.; Boo, S.; Gaynor, S. G.; Matyjaszewski, K. *Macromolecules* **1999**, *32*, 5772.
(34) Ohno, K.; Morinaga, T.; Koh, K.; Tsujii, Y.; Fukuda, T. *Macromolecules* **2005**, *38*, 2137.
(35) Robinson, K. L.; Khan, M. A.; de Paz Banez, M. V.; Wang, X. S.; Armes, S. P. *Macromolecules* **2001**, *34*, 3155.
(36) Sauerbrey, G. *Z. Phys.* **1959**, *155*, 206.
(37) Jones, D. M.; Huck, W. T. S. *Adv. Mater.* **2001**, *13*, 1256.
(38) Zhou, F.; Liu, W.; Hao, J.; Chen, M.; Liu, W.; Sun, D. C. *Chem. Lett.* **2004**, *33*, 602.
(39) Huang, W.; Kim, J.-B.; Bruening, M. L.; Baker, G. L. *Macromolecules* **2002**, *35*, 1175.
(40) Baszkin, A.; Lyman, D. J. *J. Biomed. Mater. Res.* **1980**, *14*, 393.
(41) Suttiprasit, P.; Krisdhasima, V.; Mcguire, J. *J. Colloid Interface Sci.* **1992**, *154*, 316.
(42) Carter, D. C.; He, X.-M. *Science* **1990**, *249*, 302.
(43) Hook, F.; Rodahl, M.; Brzezinski, P.; Kasemo, B. *Langmuir* **1998**, *14*, 729.
(44) Asolphi, U.; Kulicke, W.-M. *Polymer* **1997**, *38*, 1513.
(45) Liy, J. H.-Y.; Brant, D. A.; Kitamura, S.; Kajiwara, K.; Mimura, M. *Macromolecules* **1999**, *32*, 8611.
(46) Tsuruta, T. *Adv. Polym. Sci.* **1996**, *126*, 1.
(47) (a) Fujimoto, K.; Inoue, H.; Ikada, Y. *J. Biomed. Mater. Res.* **1993**, *27*, 1559. (b) Fujimoto, K.; Tadokoro, H.; Ueda, Y.; Ikada, Y. *Biomaterials* **1993**, *14*, 442.
(48) Nojiri, C.; Nakahama, S.; Senshu, K.; Okano, T.; Kawagoishi, N.; Kido, T.; Sakai, K.; Koyanagi, H.; Akutsu, T. *ASAIO J.* **1993**, *39*, 322.
(49) Nojiri, C.; Senshu, K.; Okano, T. *Artif. Organs* **1995**, *19*, 32.
(50) Senshu, K.; Yamashita, S.; Ito, M.; Hirao, A.; Nakahama, S. *Langmuir* **1995**, *11*, 2293.
(51) Senshu, K.; Yamashita, S.; Mori, H.; Ito, M.; Hirao, A.; Nakahama, S. *Langmuir* **1999**, *15*, 1754.
(52) Senshu, K.; Kobayashi, M.; Ikawa, N.; Yamashita, S.; Hirao, A.; Nakahama, S. *Langmuir* **1999**, *15*, 1763.

MA0520242

Blind Subxiphoid Pericardiotomy for Cardiac Tamponade Because of Acute Hemopericardium

Yoshihiko Kurimoto, MD, Mamoru Hase, MD, Satoshi Nara, MD, Naoya Yama, MD, Nobuyoshi Kawaharada, MD, Kiyofumi Morishita, MD, Tetsuya Higami, MD, and Yasufumi Asai, MD

Objective: **Percutaneous catheter drainage (PCD) is not always effective in a case of hemopericardium. Acute occlusion of catheter and cardiac perforation can happen more often. To perform subxiphoid pericardiotomy within a minute for emergency cases, we have done this procedure in a blind method after finger dissection by subxiphoid approach. We report the usefulness of blind subxiphoid pericardiotomy (BSP) based on the results of a prospective control study.**

Methods: **We designed a study to determine a favorable management for cardiac tamponade resulting from hemopericardium. In an emergency case of cardiac tamponade because of hemopericardium, board certified surgeons should perform BSP and other emergency physicians should perform PCD, with or without local anesthesia. PCD (n = 67) and BSP (n = 16) were performed for patients with cardio-pulmonary arrest (CPA) or near CPA because of cardiac tamponade secondary to trauma (n = 7), acute aortic dissection (n = 65), and cardiac rupture following acute myocardial infarction (n = 11) in our emergency medical center from January 2000 to December 2004.**

Results: **BSP was effective in all cases but PCD was ineffective in five cases because of clotting in pericardium ($p = 0.260$). No complication was observed in the BSP group but five critical complications and three infeasible drainage complications were observed in the PCD group ($p = 0.146$). Ten patients (BSP, 4; PCD, 6; $p = 0.077$) survived after emergency surgery (n = 8) or conservative treatment (n = 2).**

Conclusion: **BSP was safe and could be performed quickly in an emergency situation. Percutaneous catheter drainage for hemopericardium could not avoid critical complications because of clotting in pericardium.**

Key Words: **Pericardiotomy, Pericardiocentesis, Hemopericardium, Cardiac tamponade.**

J Trauma. 2006;61:582–585.

Cardiac tamponade caused by acute hemopericardium is critical and requires emergency intervention. Based on the clinical course and the findings of echo-free space in a pericardial sac, an initial treatment should be performed for relief of cardiac tamponade as early as possible. Many reports have supported the usefulness of percutaneous pericardial catheter drainage (PCD) against pericardial effusion.[1–3] PCD is less invasive, which seems preferable for severely ill patients. However, hemopericardium is different from pericardial effusion because of the possibility of clot in the pericardial sac and usually the hemopericardium becomes critical in a short period.[4,5] Conventional subxiphoid pericardiostomy overcomes some drawbacks of PCD, but requires specialized surgical instruments and takes several minutes to accomplish. We have employed subxiphoid pericardiotomy in a blind manner for selected cases with cardiopulmonary arrest (CPA) or near CPA because of cardiac tamponade caused by hemopericardium to quickly relieve the cause of CPA. In this prospective control study, we evaluate the results of blind subxiphoid pericardiotomy (BSP) for cardiac tamponade because of acute hemopericardium and compare them with the result of PCD.

Submitted for publication March 17, 2006.
Accepted for publication June 26, 2006.

From the Departments of Traumatology and Critical Care Medicine (Y.K., M.H., S.N., Y.A.), Thoracic and Cardiovascular Surgery (N.K., K.M., T.H.), and Radiology (N.Y.), Sapporo Medical University, Sapporo, Japan.
Presented as a poster at the 64th Annual Meeting of the American Association for the Surgery of Trauma September 22–24, 2005, Atlanta, Georgia.
Address for reprints: Yoshihiko Kurimoto, MD, Department of Traumatology and Critical Care Medicine, Sapporo Medical University, South 1 West 16, Chuo-ku, Sapporo 060-8543, Japan; email: kurimoto@sapmed.ac.jp.

DOI: 10.1097/01.ta.0000236060.37952.ce

METHODS

We designed a prospective control study to determine the preferred initial treatment for cases with CPA or near CPA because of cardiac tamponade caused by acute hemopericardium. In our emergency medical center, it was decided that board certified surgeons should perform BSP and other emergency physicians should perform PCD to relieve cardiac tamponade caused by acute hemopericardium. Eighty-three patients were admitted and given a diagnosis of cardiac tamponade because of acute hemopericardium as the cause of CPA or near CPA from January 2000 to December 2004. Sixty-nine patients suffered CPA during transportation to the hospital and the remaining 14 patients suffered CPA or near CPA after arrival at our emergency room. PCD (n = 67) and BSP (n = 16) were performed for patients with cardiac tamponade secondary to trauma (n = 7), acute aortic dissection (n = 65) and cardiac rupture after acute myocardial infarction (n = 11). There was no difference statistically between the two groups (Table 1).

BSP

Most patients had been undergoing cardiopulmonary resuscitation (CPR) with tracheal intubation before or during BSP. A 5 cm-long skin incision is made from the lower end

Table 1 Patients' Characteristics

	No.	Age	Male/ Female	Trauma/ AD/MI	CPAOA/ CPAAA
PCD	67	70.4 ± 15.7	30/37	6/54/7	59/8
BSP	16	66.5 ± 16.4	9/7	1/11/4	10/6

PCD, percutaneous pericardial catheter drainage; BSP, blind subxiphoid pericardiotomy; AD, aortic dissection; MI, myocardial infarction; CPAOA, cardiopulmonary arrest on arrival; CPAAA, cardiopulmonary arrest (or near CPA) after arrival.

of the sternum caudally. The upper linea alba is divided in the midline without resection of the xiphoid sternum (Fig. 1A). The tissue plane between the posterior wall of the sternum and the anterior pericardium is developed by blunt finger dissection without any specific surgical instrument (Fig. 1B). While touching the pericardium with an index finger, an inferior site of the pericardium is cut by scissors (Fig. 1C). If cardiac tamponade is not quickly relieved by pericardiotomy, clots in the pericardium are evacuated using a suction system. In cases in which spontaneous circulation is restored, a drainage tube (20–28 Fr.) is placed in the pericardium (Fig. 1D) and a skin incision is approximated temporarily to transport patients to an operating room if indicated.

Percutaneous Pericardial Catheter Drainage

Most patients had been undergoing CPR with tracheal intubation before or during PCD. After confirmation of distance and direction from the subxiphoid access site to the pericardium using echocardiography, the pericardium is entered with an 18-gauge needle by a standard subxiphoid approach. A 0.035-in (0.089 cm) J tip guide wire is advanced into the pericardial space and the needle removed. The tract of the needle is dilated with an 8.5 Fr. dilator, and an 8.5 Fr. pericardial catheter (Pericardiocentesis set, Cook Inc., Bloomington, IL) is advanced into the pericardial space. In cases in which spontaneous circulation is restored, patients are transported to an operating room if indicated.

Statistical Analysis

The data are presented as means ± SD. The Mann-Whitney U test or the χ^2 test was used to compare data in the two groups using the statistical software program StatView-J 5.0, (SAS Institute Inc., Cary, N.C.).

RESULTS

BSP was effective in all cases but PCD was ineffective in five cases because of clotting in the pericardium ($p = 0.260$). Ten patients (BSP, 4; PCD, 6; $p = 0.077$) survived after emergency surgery (n = 8) or conservative treatment (n = 2). No complication was observed in the BSP group but there were five critical complications and three infeasible drainage complications in the PCD group ($p = 0.146$) (Fig. 2). Right ventricular puncture (n = 2) caused by PCD resulted in one death and one open repair after BSP as a second intervention. Acute occlusion of percutaneous drainage tube (n = 3) resulted in two deaths and one emergency thoracotomy (Table 2).

DISCUSSION

Many reports have discussed methods to relieve cardiac tamponade, but mainly in elective cases caused by pericardial effusion.[1–3,6–11] Representative methods of initial management are percutaneous pericardial catheter drainage (PCD)

Fig. 1. *Operative procedure of BSP. The linea alba is divided* (A). *After blunt finger dissection* (B), *the pericardium is cut by scissors* (C). *A drainage tube is placed in the pericardium* (D).

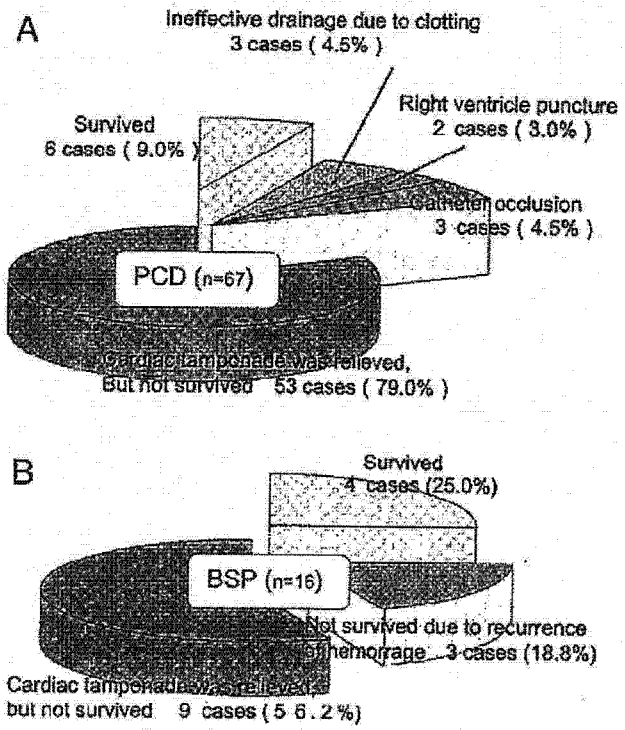

Fig. 2. *Results of percutaneous pericardial catheter drainage (A) and BSP (B). BSP was effective in all cases but PCD was ineffective in five cases (p = 0.260). Ten patients survived (BSP, 4; PCD, 6; p = 0.077). No complication was observed in the BSP group but there were five critical complications and three infeasible drainage complications in the PCD group (p = 0.146).*

Table 2 Clinical Course of Patients With Complications After PCD

Infeasible drainage (n = 3)	67-yr-old woman with AD died in the ER
	55-yr-old man with MI subsequently underwent BSP died in the ER
	69-yr-old man with MI subsequently underwent ERT died in the ER
RV puncture (n = 2)	76-yr-old woman with AD subsequently underwent BSP in the ER, and survived after open repair in the OR
	72-yr-old woman with MI subsequently underwent BSP in the ER, but died during transportation to the OR
Occlusion of catheter (n = 3)	19-yr-old man with trauma subsequently underwent BSP in the ER, and survived after open repair in the OR
	62-yr-old man with MI subsequently underwent BSP in the ER, but died during preparation of open repair in the ICU
	65-yr-old woman with AD died in the ICU

PCD, percutaneous pericardial catheter drainage; AD, aortic dissection; ER, emergency room; MI, myocardial infarction; BSP, blind subxiphoid pericardiotomy; ERT, emergency room thoracotomy; OR, operating room; ICU, intensive care unit.

and subxiphoid pericardiostomy. Three decades ago, needle pericardiocentesis was performed at the bedside without echocardiographic guidance or hemodynamic monitoring and the risk of life-threatening complications were as high as 20%.[4] However, the Mayo clinic group reported that echocardiographically guided pericardiocenteses could be performed with a total complication rate of 4.7% (major, 1.2%; minor, 3.5%)[2] and Maggiolini et al. reported that it could be done more safely using a probe-mounted needle.[1] On the other hand, some reports have presented better results of subxiphoid pericardiostomy as a method of managing pericardial effusion, not only to relieve cardiac tamponade but also for diagnosis of malignancy and infection.[7–9] Regarding the drawbacks of subxiphoid pericardiostomy, it usually requires general anesthesia and surgically trained (to some extent) physicians and it takes several minutes to perform. According to studies comparing these two methods, subxiphoid pericardiostomy was preferable for elective cases with pericardial effusion and PCD should be employed for emergency cases because of cardiac tamponade.[10,11]

The present study was designed to evaluate our modified subxiphoid pericardiotomy, employed to overcome some of the drawbacks of these two techniques for emergency cases with cardiac tamponade secondary to hemopericardium. Echo-guided PCD can be done immediately in the emergency room and also completely avoids the critical complication of right ventricle puncture if using a special needle carrier that facilitates continuous visualization during pericardial puncture. Nevertheless, needle aspiration cannot guarantee that intrapericardial blood will be successfully drawn in a case of clotting hemopericardium.[4] In such cases, it might often result in not only ineffective pericardial drainage but also right ventricle puncture. On the other hand, conventional subxiphoid pericardiostomy generally demands specialized surgical instruments and can be too time-consuming for emergency cases, such as our present CPA cases. Our modified pericardiotomy guarantees relief of cardiac tamponade secondary to hemopericardium and can be performed in a minute without specialized surgical instruments even during cardiac massage, which seems to be preferable for emergency cases, such as CPA or near CPA.

In cases of acute pericardial hemorrhage after trauma, surgical repair of cardiac injury has been recommended as the definitive treatment.[5,12,13] In particular, patients with penetrating cardiac injury need to be transferred to the operating room after or even before pericardial drainage. However, considering that there was a report of percutaneous catheter pericardial drainage being effective in all cases with hemopericardium,[14] it might be reasonable to observe patients with blunt cardiac injury concomitant with other critical injuries and to only perform PCD to relieve cardiac tamponade. In our department, surgical or cath-

eter pericardial drainages have not been employed in the emergency room for patients with acute hemopericardium whose hemodynamics do not contraindicate transfer to the operating room. However, in cases of CPA because of hemopericardium, pericardial drainage is mandatory to resuscitate those patients. In such a situation, we think that pericardial drainage, especially blunt subxiphouid pericardiotomy, must be the first choice of management before emergency room thoracotomy.[15] In the operating room, median sternotomy allows various kinds of repair of cardiac injury. However, although there are insufficient surgical instruments and no circulation assist system in the emergency room, the color of blood gained by pericardial drainage might provide valuable information about the site of cardiac injury, which might suggest the preferable procedure to be undertaken in the emergency room (median sternotomy or left antero-lateral thoracotomy) for patients who cannot be transferred to the operating room even after pericardial drainage.[16]

Although we have to consider a possible bias in this study because only board certified surgeons performed blind subxiphoid pericardiotomy and because of the limited number of patients, our modified pericardiotomy seems to be safe and effective for emergency hemopericardium. In conclusion, blunt subxiphoid pericardiotomy could be a treatment of choice for critical acute hemopericardium. Percutaneous catheter drainage for hemopericardium could not avoid critical complications because of clotting in the pericardium in some cases.

REFERENCES

1. Maggiolini S, Bozzano A, Russo P, et al. Echocardiography-guided pericardiocentesis with probe-mounted needle: report of 53 cases. *J Am Soc Echocardiogr.* 2001;14:821–824.
2. Tsang TS, Enriquez-Sarano M, Freeman WK, et al. Consecutive 1127 therapeutic echocardiographically guided pericardiocenteses: clinical profile, practice patterns, and outcomes spanning 21 years. *Mayo Clin Proc.* 2002;77:429–436.
3. Marcy PY, Bondiau PY, Brunner P. Percutaneous treatment in patients presenting with malignant cardiac tamponade. *Eur Radiol.* 2005;15:2000–2009.
4. Wong B, Murphy J, Chang CJ, et al. The risk of pericardiocentesis. *Am J Cardiol.* 1979;44:1110–1114.
5. Duncan AO, Scalea TM, Sclafani SJ, et al. Evaluation of occult cardiac injuries using subxiphoid pericardial window. *J Trauma.* 1989;29:955–959.
6. Kabukcu M, Demircioglu F, Yanik E, et al. Pericardial tamponade and large pericardial effusions. *Tex Heart Inst J.* 2004;31:398–403.
7. Palantianos GM, Thurer RJ, Pompeo MQ, et al. Clinical experience with subxiphoid drainage of pericardial effusions. *Ann Thorac Surg.* 1989;48:381–385.
8. Dosios T, Theakos N, Angouras D, et al. Risk factors affecting the survival of patients with pericardial effusion submitted to subxiphoid pericardiostomy. *CHEST.* 2003;124:242–246.
9. Becit N, Unlu Y, Ceviz M, et al. Subxiphoid pericardiostomy in the management of pericardial effusions: case series analysis of 368 patients. *Heart.* 2005;91:785–790.
10. Allen KB, Faber LP, Warren WH, et al. Pericardial effusion: subxiphoid pericardiostomy versus percutaneous catheter drainage. *Ann Thorac Surg.* 1999;67:437–440.
11. McDonald JM, Meyers BF, Guthrie TJ, et al. Comparison of open subxiphoid pericardial drainage with percutaneous catheter drainage for symptomatic pericardial effusion. *Ann Thorac Surg.* 2003;76:811–816.
12. Harris DG, Papagiannopoulos KA, Pretorius J, et al. Current evaluation of cardiac stab wounds. *Ann Thorac Surg.* 1999;68:2119–122.
13. Navsaria PH, Nicol AJ. Haemopericardium in stable patients after penetrating injury: is subxiphoid pericardial window and drainage enough? A prospective study. *Injury.* 2005;36:745–750.
14. Symbas PN, Diorio DA, Tyras DH, et al. Penetrating cardiac wounds. *J Thorac Cardiovasc Surg.* 1973;66:526–532.
15. Naunheim KS, Kesler KA, Fiore AC, et al. Pericardial drainage: subxiphoid vs. transthoracic approach. *Eur J Cardio-thorac Surg.* 1991;5:99–104.
16. Sugimoto S, Yamashita A, Baba M, et al. Pericardial drainage prior to operation contributes to surgical repair of traumatic cardiac injury. *Jpn J Thorac Cardiovasc Surg.* 1999;47:31–35.

胸部外科の指針

討論
1. 金子達夫
2. 中野穣太

高リスク例に対するOPCAB

花田智樹　樋上哲哉　金築一摩　清水弘治
今井健介　本多　祐　菊地慶太*

はじめに

冠状動脈疾患例において，高齢化および冠状動脈インターベンションの発展などに伴い，冠状動脈バイパス術（CABG）を要する対象は合併疾患を有する症例が多くを占めるにいたり，いわゆる高リスク例に対する完全冠血行再建の必要性が増大してきている．一方，近年off-pump CABG（OPCAB）の手技の定型化および安全性の向上に伴い，より低侵襲での完全冠血行再建が可能となった．当施設では，単独CABG対象例においては原則としてOPCABを第一選択としている．本研究では，高リスク例に対するOPCABの早期成績からこのような症例におけるOPCABの適応およびグラフト選択を含む手技の安全性・妥当性を評価することを目標とした．

I. 対象および方法

最近2年間に行った単独OPCAB連続110例［小切開CABG（MIDCAB）を除く］を対象とした．平均年齢70.9±8.7（51～90）歳，男性77例，女性33例であった．

対象例のうち脳血管障害（脳梗塞既往，内頸動脈狭窄など），超高齢（80歳以上），腎機能障害（CRE 2.0 mg/dl以上），低左心機能［左室駆出率（EF）40%未満］，糖尿病（インスリン使用），呼吸機能低下（1秒率50%未満），緊急手術（24時間以内），急性心筋梗塞，術前からの大動脈内バルーンパンピング（IABP）あるいは経皮的心肺補助装置（PCPS）の使用を危険因子とし，この有無によって2群に分けて検討した．術前にこれらの危険因子を有する68例を高リスク群（H群），危険因子のない42例を低リスク群（L群）とした．

患者背景を表1に示す．男女比，平均病変枝数

表1．患者背景

	H群（n=68）	L群（n=42）	p値
平均年齢（歳）	73.0±8.6	67.5±8.0	0.0012
症例数（男/女）	46/22	31/11	NS
平均病変枝数	2.5±0.6	2.4±0.6	NS
Euro score	7.3±3.2	2.9±2.1	<0.0001

表2．H群（n=68）における危険因子

	症例数（%）
脳血管障害	30（44.1）
超高齢（≧80歳）	18（26.5）
糖尿病（インスリン使用）	16（23.5）
腎機能障害（CRE≧2.0 mg/dl）	15（22.1）
低左心機能（EF<40%）	15（22.1）
呼吸機能低下（1秒率<50%）	2（2.9）
緊急手術	12（17.6）
急性心筋梗塞	6（8.8）
術前IABP	14（20.6）
術前PCPS	1（1.5）

キーワード：ハイリスク例，OPCAB

* T. Hanada（講師），T. Higami（教授），K. Kanetsuki，K. Shimizu，K. Imai，T. Honda，K. Kikuchi（講師）：島根大学循環器・消化器総合外科．

表 3. 手術結果

	H 群(n=68)	L 群(n=42)	p 値
平均グラフト枝数	2.9±0.9	2.9±0.9	NS
術中 IABP 使用	0	0	NS
on-pump beating CABG への convert	1	0	
完全血行再建率(%)	85	93	NS
各種グラフト使用率(%)			
LITA	93	100	NS
RITA	82	88	NS
RGEA	50	38	NS
RA	0	2	NS
領域別平均吻合数			
LAD	1.19	1.40	NS
LCx	1.14	0.92	NS
RCA	0.55	0.47	NS
sequential バイパス施行率(%)	48	60	NS

LITA：左内胸動脈，RITA：右内胸動脈，RGEA：右胃大網動脈，RA：橈骨動脈，LAD：左前下行枝，LCx：左回旋枝，RCA：右冠状動脈

表 4. 術後経過

	H 群(n=68)	L 群(n=42)	p 値
グラフト開存率(%)	100.0(n=56)	97.1(n=34)	NS
病院死亡	1 例(1.5%)	0	
術後合併症(例)			
脳梗塞	0	0	
腎不全の悪化(透析)	1(1.5%)*	0	
肺炎	1(1.5%)	0	
呼吸不全(挿管 10 日以上)	1(1.5%)*	0	
周術期心筋梗塞	1(1.5%)	1(2.4%)	
縦隔洞炎	0	2(4.8%)	

*同一症例

では両群間に有意差はなかったが，H 群は L 群より有意に高齢であり（p=0.0012），また Euro score も H 群が L 群に対して有意な高値を示した（p<0.0001）．

H 群における危険因子の内訳を表 2 に示す．脳血管障害例では脳梗塞の既往 16 例（53%），総頸動脈あるいは内頸動脈の 50% 以上狭窄 5 例（17%），両方とも認めるもの 9 例（30%）であった．また，腎機能低下例のうち 10 例（67%）は慢性透析患者であった．

II. 手術方法

手術では ultrasonic complete skeletonization (UCS) 法により左右の内胸動脈と右胃大網動脈を採取した．一部の症例では橈骨動脈も使用した．体位は右下 Trendelenburg 位とし，原則として 3 針の Lima suture のみにて心臓を脱転した．心臓の脱転位をかえることなくスタビライザーを用いて吻合部の固定が可能であり，すべての吻合を同一心臓位で完了しえた．グラフト吻合時にはシャントチューブを使用し，動脈吻合のすべてを 8-0 ポリプロピレンの連続縫合とした．原則として可及的に *in situ* 動脈グラフトとし，aortic no-touch にて完全血行再建を行った．このさい，多枝バイパスでは sequential バイパスを積極的に用いた．

統計処理は Student t 検定，χ^2 検定を用い，p<0.05 を有意とした．数値は平均値±標準偏差で示した．

III. 結　　果

平均グラフト枝数は両群間で有意差を認めなかった．術中に IABP が新たに必要となった症例はなく，H 群の 1 例（術前左心機能は良好）で，吻合中に心電図上 ST が低下したために on-pump beating CABG への convert が必要であった．H 群の 2 例，L 群の 1 例に腹部大動脈瘤に対する人工血管置換術を同時に行った．完全血行再建率は H 群 85%，L 群 93% と，両群間で有意差はなかった．各種グラフト使用率，領域別平均吻合数，sequential バイパス施行率にも両群間で有意差はなかった（表 3）．

術後の冠状動脈造影は H 群 56 例（82%），L 群 34 例（81%）に行い，グラフト開存率は H 群 100%，L 群 97.1% と両群間で有意差はなかった．病院死亡は H 群の 1 例（1.5%）のみで，術後 3 日に不整脈によると思われる突然死にて失った．H 群において，術前にショック状態であった 1 例で腎不全が悪化して慢性透析が必要となり，さらに術後 10 日以上の人工呼吸器管理が必要であった．軽度の周術期心筋梗塞を両群に 1 例ずつ認めたが，CPK や CPK-MB の上昇のみで

血行動態には異常を認めなかった．肺炎をH群で1例，縦隔洞炎をL群で2例認めたが，術後に脳梗塞を生じた症例は両群ともになかった（表4）．以上，なんらかの合併症を発症した症例はH群5例（7.4%），L群3例（7.1%）であった．

IV. 考　　察

近年，社会の高齢化が進展するとともに高齢者に対するCABGの必要性が増大してきている．本研究の対象症例に占める80歳以上の超高齢者の割合は16.4%であり，本邦報告例（2.7～4.1%）[1~3]と比較しても高齢者の比率が高かった．高齢者では動脈硬化がより進行しているため，脳血管障害などの手術危険因子を有している可能性が高く，また急性心筋梗塞など緊急手術が必要となることも多い[2,4]．一方，CABGにおいては近年OPCABの適応が拡大し，成績も安定してきた．Wanら[5]は，人工心肺を使用したconventional CABG（C-CABG）と比較してOPCABではサイトカインの反応や心筋障害が少ないと述べ，Sabikら[6]はOPCABにより完全血行再建率は低下したものの術後の合併症が減少したことを報告した．

以上の経緯を踏まえ，本研究ではH群に対してOPCABを選択する妥当性を明らかにするために，その早期成績を同時期に行ったL群と比較・検討した．

本研究では脳血管障害，超高齢，腎機能障害，低左心機能，糖尿病，呼吸機能低下，緊急手術，急性心筋梗塞，術前からのIABPあるいはPCPSの使用を危険因子とした．手術危険率を予測するEuro score[7]を適用してみると，H群はL群よりも有意に高値であり，2倍以上のscoreであった．このことからも，本研究におけるH群は一般的にもかなりの手術危険率を有するものと考えられる．

人工心肺を使用するC-CABGのもっとも大きな合併症は周術期に発症する脳血管障害であるが，これは上行大動脈の動脈硬化が主な原因とされる[8]．C-CABGと比べOPCABでは送血管の挿入や上行大動脈の遮断が必要ないため，これらの操作により脳塞栓を生ずる危険性はなく，また自己心拍による拍動流によって灌流されるため，低灌流による脳梗塞の発症も回避することができる．このため，C-CABGと比較してOPCABでは術後の脳血管障害が減少する[9]．本研究においてもH群における術前危険因子では脳血管障害がもっとも多く，約半数の症例に認めたにもかかわらず，術後に脳梗塞を新たに発症した症例はなかった．当科では可及的に動脈グラフトのみを用いた*in situ*での血行再建を行っており，人工心肺を使用しないことに加えaortic no-touchにてOPCABを行っていることが，脳塞栓の高リスク例においても脳合併症を回避できた要因と考えられる．

腎機能が低下した症例や慢性透析患者において，人工心肺を使用しないOPCABは術中・術後の水分管理が容易である[10]．橈骨動脈をグラフトとして使用できないことに対しては，UCS法で採取したグラフトは使用できる距離が長いため[11]，sequentialバイパスを積極的に行うことで，両側内胸動脈や右胃大網動脈という*in situ*動脈グラフトのみによる血行再建が可能であった．遠隔期の開存率に問題のある静脈グラフトを使用する必要性は生じなかった．

OPCABでは心臓の脱転やスタビライザーでの圧迫などにより血行動態の悪化を生ずることが懸念される[9,12]が，われわれは冠状動脈吻合時に手術台を傾け，右下Trendelenburg位とし前負荷を増加させることにより，血行動態の変化を最小限に抑えた．また，この体位でLima sutureを3針かけて牽引すると自然に心尖部が挙上するため，スタビライザーで過度に心臓を圧迫することなく良好な視野を確保することが可能であった．吻合中は冠状動脈内シャントチューブを使用し，末梢への血流を維持するように努めた．吻合時に心電図上STが低下した1例でon-pump beating CABGへのconvertが必要であったが，急性心筋梗塞やEF 40%以下の左心機能低下例でもoff-pumpにてCABGを完遂することができた．

本研究ではバイパス本数にH群，L群間で差は認めなかった．また，使用したグラフトの種類や末梢吻合の領域についても両群間で大きな差はなかった．Sequentialバイパス施行率，完全血

行再建率はL群で高い傾向にあったが有意差はなく，また術後早期のグラフト造影ではL群の開存率が97.1%であったのに対し，H群では全例開存していた．これらの結果は，H群においてもL群と同様のクオリティの手術を行いうることを示すものと考えられる．

病院死亡はH群に1例認めた．急性心筋梗塞にて緊急手術を行った症例で術後経過は良好であったが，術後3日に一般病棟にて不整脈が原因と思われる突然死で失った．術後の合併症については症例数が少ないため正確な比較はむずかしいが，L群と比較してH群で合併症が増加することはなかった．諸家の報告でも，Carrierら[13]は無作為試験を行い，高リスク例ではC-CABGと比較しOPCABで術後の合併症が少ないことを示した．またAromら[14]は，とくに高リスク例において死亡率が有意に改善したことを報告した．当施設ではCABGを原則としてすべてOPCABで行っているためC-CABGとの比較はできないが，合併症の頻度がL群とほぼ同等であったことは，H群における術中・術後の合併症を回避するうえでOPCABが非常に有用であることを示唆している．

社会の高齢化は加速しており，高リスク例に対するOPCABの必要性は今後さらに増大していくと思われる．本研究ではすべて*in situ*動脈グラフトを用いることにより，H群に対してもL群と同様のクオリティにて安全に冠血行再建を行いうることが示唆された．今回は術後の早期成績について検討したが，遠隔成績や個々の危険因子についてのさらなる検討が必要である．

おわりに

高リスク例に対するOPCABの成績は良好であり，とくに脳血管障害を有する症例にはきわめて有用と考えられた．高リスク例においても安全に*in situ*動脈グラフトにて血行再建を行うことが可能であった．

文　献

1) 杉本　努，山本和男，田中佐登司ほか：超高齢者（80歳以上）におけるCABG．胸部外科 58：96-101, 2005
2) 大木　茂，金子達夫，佐藤泰史ほか：超高齢者（80歳以上）に対する冠状動脈バイパス術の検討．胸部外科 55：829-836, 2002
3) 向井資正，村田紘崇，上田哲也ほか：高齢者（80歳以上）に対する冠状動脈バイパス術の検討．胸部外科 50：653-655, 1997
4) Peterson ED, Cowper PA, Jollis JG et al：Outcomes of coronary artery bypass graft surgery in 24,461 patients aged 80 years or older. Circulation 92[Suppl 2]：85-91, 1995
5) Wan S, Izzat MB, Lee TW et al：Avoiding cardiopulmonary bypass in multivessel CABG reduces cytokine response and myocardial injury. Ann Thorac Surg 68：52-57, 1999
6) Sabik JF, Gillinov AM, Blackstone EH et al：Does off-pump coronary surgery reduce morbidity and mortality? J Thorac Cardiovasc Surg 124：698-707, 2002
7) Nashef SAM, Roques F, Michel P et al：European system for cardiac operative risk evaluation (Euro score). Eur J Cardiothorac Surg 16：9-13, 1999
8) Roach GW, Kanchuger M, Mangano CM et al：Adverse cerebral outcomes after coronary bypass surgery. N Engl J Med 335：1857-1863, 1996
9) 平手博之，井村奈美，土井るみなほか：Off-pump CABGと従来のCABGの周術期諸因子の比較．麻酔 53：252-257, 2004
10) Hirose H, Amano A, Takahashi A：Efficacy of off-pump coronary artery bypass grafting for the patients on chronic hemodialysis. Jpn J Thorac Cardiovasc Surg 49：693-699, 2001
11) Higami T, Kozawa S, Asada T et al：Skeletonization and harvest of the internal thoracic artery with an ultrasonic scalpel. Ann Thorac Surg 70：307-308, 2000
12) Heames RM, Gill RS, Ohri SK et al：Off-pump coronary artery surgery. Anaesthesia 57：676-685, 2002
13) Carrier M, Perrault L, Jeanmart H et al：Randomized trial comparing off-pump to on-pump coronary artery bypass grafting in high-risk patients. Heart Surg Forum 6：E89-E92, 2003
14) Arom KV, Flavin TF, Emery RW et al：Safety and efficacy of off-pump coronary artery bypass grafting. Ann Thorac Surg 69：704-710, 2000

SUMMARY Off-pump Coronary Artery Bypass in High-risk Patients

Tomoki Hanada et al., Department of Cardiovascular and General Surgery, School of Medicine, Shimane University, Izumo, Japan

In this study, 110 consecutive patients who had undergone off-pump coronary artery bypass (OPCAB) in the past 2 years were evaluated for early results of OPCAB. Patients were classified as a high-risk group (H group : 68 patients consisting of 46 men and 22 women) and a low-risk group (L group : 42 patients consisting of 31 men and 11 women), respectively, and were evaluated for the early operative results. No differences were noted between the H and L groups in the mean number of bypass grafts (2.9±0.9 in the H group, 2.9±0.9 in the L group), the rates of complete revascularization (85% in the H group, 93% in the L group), those of various graft materials bypassed, or those of sequential bypass. In all patients, we were able to undergo coronary revascularization by the aortic no-touch technique using arterial grafts exclusively. In the H group, 1 patient (1.5%) died in hospital, but no patients developed cerebral infarction postoperatively, and the frequency of complications was similar to that in the L group. The results of OPCAB for high-risk patients were good, and it was suggested that OPCAB using *in situ* arterial grafts was very useful particularly in patients with cerebrovascular diseases.

KEY WORDS : high-risk patient/OPCAB

討論 1.

金子達夫*

2年間の単独off-pump冠状動脈バイパス術(off-pump CABG：OPCAB)例連続110例を対象とした，リスクによる分類での指針論文を拝読した．まず死亡1例，合併症をすべて含めて8例という手術成績に敬意を表するものである．この要因として*in situ*動脈グラフトを使用したOPCABが大きな関与をしていることは否めない．すなわち人工心肺を使用せず，中枢吻合を必要としない手術手技が安全に行われた結果であろう．

この成績を踏まえたうえで，花田らの述べた高リスク例について検討してみたい．まず，80歳以上の症例の占める割合が16.4%と非常に高いのはなぜであろうか．人口構成比やバイパス術の平均年齢からしても多少の違和感を覚える．また，花田らの定義する高リスクには，脳梗塞既往例や50%以上の頸動脈狭窄，腎機能障害がCRE 2.0 mg/dl以上，左室駆出率(EF) 40%未満の低左心機能，インスリン使用の糖尿病，1秒率50%未満など，一般的にはさほど高リスクと考えられない事項が列挙され，その結果として高リスク例が62%(110例中68例)と過半数を超える高値となってしまっていることに注目したい．これらのうちで真に高リスクと考えられるのは，75%以上の頸動脈狭窄，合併症を伴った超高齢者，透析例，緊急手術，急性心筋梗塞，経皮的心肺補助装置(PCPS)以上の左室補助を伴う症例などではないであろうか．日本胸部外科学会の2003年レポートでは，緊急手術と再バイパス術および透析例が高死亡率として報告されている[1]．リスクの階層化にEuro scoreは有用であり，花田らの結果でも高リスク例では術後合併症が高率である．

手術手技については，左右内胸動脈と胃大網動脈をUCS法で採取し，Lima stitchとスタビライザーによるシャントチューブ使用下のOPCABで，大動脈に触れずにバイパス術を行っており，問題となる点は見当たらない．ただ，1例のみ吻合中にST低下がみられ人工心肺を使用したのはなぜであろうか．また，採取グラフトの距離が長いのでsequentialバイパスを多用しているとのことであるが，吻合個所は増えるがTあるいはY型グラフトによるバイパスのほうが技術的に容易な場合もあるかもしれない．しかし，いずれにせよ動脈グラフトによる*in situ*バイパスを主

* T. Kaneko (副院長)：群馬県立心臓血管センター(〒371-0004 前橋市亀泉町甲3-12)．

体としている点は筆者も賛成である．

また完全血行再建について，花田らは高リスク例では必要であると述べている．リスクをもつ患者に対しあえて完全血行再建をめざすのであれば，一般的には手術リスクはさらに増すのではないであろうか．高リスク例ではあえて完全再建にこだわらず，キーベッセルにバイパスをおき他はハイブリッドあるいは内科治療にゆだねる症例もあるのではないかと思われる．もちろん，無理なく完全血行再建ができるのであればそれに越したことはないであろうが．

OPCABに関しては徐々に適応が拡大され，本邦における2003年のCABG例の半数以上がこれによると報告[1]されている．この点について筆者の現在の考えは，まずはじめにOPCABありきではなく，質の高い，すなわち動脈グラフトによる安全なバイパスを行うことが可能であれば行うべきで，最初からOPCABにこだわる必要はないのではないかということである．大動脈硬化でも術中エコーを使用して安全な場所を選択すれば人工心肺が可能な場合が多く，80歳以上の超高齢者でも70歳台のconventional CABG (C-CABG) と比較して安全に施行可能であった[2]．本論文とは関係ないが，OPCABであるがゆえに静脈グラフトとしたり，冠状動脈末梢の遠位部で縫合せざるをえなくなるのは本末転倒ではないであろうか．また，術中にST低下や不整脈の出現，さらには血圧の低下を招いてまで手術を遂行し，その結果大動脈内バルーンパンピング (IABP) やPCPSなどの補助循環が必要になったという話も耳にする．あるいは径1 mmの吻合を拍動下で行うのと静止野で行うのでは，おのずと縫合の質に差が生ずるのではないであろうか．本論文ではそれらの点について述べられていないが，この間のon-pump例はいかほどあったのであろうか．たしかにOPCABは低侵襲であることは論をまたない．しかし，手術に求められるのは侵襲に見合った結果である．手術の侵襲度からいえばOPCABといえどもカテーテル治療とは比較にならないはずで，薬剤溶出ステント (DES) の出現以来バイパス数は世界的に減少し，本邦でも2003年にそれまで右肩上がりであった虚血手術ははじめて低下をきたした．考えるべきはまず手術の安全と患者の術後長期QOL向上をめざした手術で，次の手段としてon-pumpかoff-pumpの選択となるのではないかと筆者は考える．

最後に，高リスクの患者にどのようなバイパス術を行うべきかという点について簡単に言及したい．頸動脈狭窄への対策としては，同時手術と待期手術の選択問題がある．高齢者と透析例では個々の症例で石灰化の位置などを把握したうえでグラフト選択を行い，完全血行再建に拘泥せずに対応すべきと考える．急性心筋梗塞と緊急例では手術成績が不良であるため，さらに慎重な適応と術式への配慮が必要となる．しかし，補助循環を行っている症例はon-pump beatingとかわらないので，そのまま心拍動下でも手術可能であろう．

文　献

1) Kazui T, Wada H, Fujita H：Thoracic and cardiovascular surgery in Japan during 2003；annual report by the Japanese Association for Thoracic Surgery. Jpn J Thorac Cardiovasc Surg 53：517-536, 2005
2) 大木　茂，金子達夫，佐藤泰史ほか：超高齢者（80歳以上）に対する冠状動脈バイパス術の検討．胸部外科 55：829-836, 2002

討論2.　中野穣太　岡林　均*

本論文では，脳血管障害など高リスク患者に対してoff-pump冠状動脈バイパス術（off-pump CABG：OPCAB）を安全に施行しえた結果が示された．ここでは三つの課題について述べたい．

一つは高リスクの定義の問題である．Euro scoreが7.3と高い値となっているため全体として問題ないと考えるが，CREの値や低左心機能の定義などがEuro scoreのものとはずれており，また経皮的心肺補助装置（PCPS）使用下のCABGはOPCABではないのかと考える．実際，今回の定義と併せて考えると，当科で2000～2005年にかけて施行したOPCABの1,500例中，771例（51.4%）と過半数が高リスクとなる．たとえばEuro score何点以上を高リスクとしたという定義のほうが鮮明となるし，他施設との比較も容易になると考える．また，急性心筋梗塞でポンプ失調をきたし，大動脈内バルーンパンピング（IABP）のみならずPCPS使用が必要となる症例はわれわれも経験しているが，これはPCPSというポンプ補助を行っているため，術前状態を含めOPCABとは分けて考える必要がある．

次にグラフト選択についてであるが，ほとんどの症例で両側内胸動脈と右胃大網動脈を用いてバイパスを行っているが，完全血行再建率が高リスク群で85%，低リスク群で93%とやや低値である．CABGはpalliative operationであることを考えるならば完全血行再建をめざすべきとわれわれは考えており，当科では96.4%に完全血行再建を行い，平均末梢吻合箇所は3.7ヵ所であった．また，とくに狭窄の程度の軽い右冠状動脈に対しては，右胃大網動脈ではcompetitionを起すことがあるため，大伏在静脈か橈骨動脈によるACバイパスがよいと考える．

最後に周術期合併症であるが，本研究にあるようにOPCABの場合，人工心肺を用いたCABGに比して減少することが明らかとなってきた．とくに脳障害は，Lundらの報告にもあるようにoff-pumpで施行することで減少することが示された[1]．しかし，Likoskyらが指摘するように周術期脳障害は術中の要素と術後の要素とを分けて考える必要があり[2]，当科でも1,500例中21例の周術期脳障害を経験しており，そのうち17例は遅発性脳障害であった．つまり，人工心肺を使用せず，aortic manipulationを行わないことで術中脳障害は回避できるが，術後遅発性脳障害は起りうる．この原因の一つとしては心臓手術後の過凝固が考えられ，当科では現在heparin calciumの予防的投与を行っている．

以上三つの課題を述べてきたが，全体として高リスク例に対してバイパス開存率，合併症，死亡率含め問題ない結果を提示されており，今後も遠隔期を含めた高リスク例に対する報告を行っていただきたい．

文　献

1) Lund C, Hol PK, Lundblad R et al：Comparison of cerebral embolization during off-pump and on-pump coronary artery bypass surgery. Ann Thorac Surg 76：765-770, 2003
2) Likosky DS, Leavitt BJ, Marrin CA et al：Intra-and postoperative predictors of stroke after coronary artery bypass grafting. Ann Thorac Surg 76：428-434, 2003

* J. Nakano, H. Okabayashi（副院長）：小倉記念病院心臓血管外科（〒802-8555 北九州市小倉北区貴船町1-1）．

Gas Exchange

Development of an Implantable Oxygenator with Cross-Flow Pump

YUICHI ASAKAWA,* AKIO FUNAKUBO,* KAZUYOSHI FUKUNAGA,† ICHIRO TAGA,† TETSUYA HIGAMI,‡ TSUYOSHI KAWAMURA,§ AND YASUHIRO FUKUI*

Thrombogenicity, a problem with long-term artificial lungs, is caused by blood-biomaterial interactions and is made worse by nonuniform flow, which also causes decreased gas exchange. To overcome these obstacles, we changed the inlet and added a uniform flow pump to our previous oxygenator design. Conventional membrane oxygenators have a ½-inch port for the inlet of blood. These port structures make it difficult for the blood to flow uniformly in the oxygenator. In addition, the complex blood flow patterns that occur in the oxygenator, including turbulence and stagnation, lead to thrombogenicity. A cross-flow pump (CFP) can result in uniform blood flow to the inlet side of an oxygenator. In this study, we evaluated the usefulness of an integrated oxygenator with a fiber bundle porosity of 0.6 and a membrane surface area of 1.3 m^2. The inlet part of the oxygenator is improved and better fits the outlet of the CFP. Each of the three models of the improved oxygenator has a different inlet taper angle. The computational fluid dynamics analysis showed that, compared with the original design, uniform flow of the integrated oxygenator improved by 88.8% at the hollow fiber membrane. With the integrated oxygenator, O_2 transfer increased by an average of 20.8%, and CO_2 transfer increased by an average of 35.5%. The results of our experiments suggest that the CFP, which produces a wide, uniform flow to the oxygenator, is effective in attaining high gas exchange performance. *ASAIO Journal* 2006; 52:291–295.

Lung transplant is the treatment of last resort for patients with respiratory failure. Unfortunately, in many cases, patients have to wait a long time for a lung transplant because of a lack of donor lungs. Thus, an artificial implantable lung is a useful respiratory support device for patients with severe lung failure awaiting lung transplantation. We have developed two types of artificial implantable lungs (AIL). The pumpless AIL was designed using a multiobjective genetic algorithm.[1] However, an AIL with a blood pump is also required for patients who need circulatory support.[2–4] The right ventricle might develop cardiac failure due to the resistance created by the oxygenator if an implantable oxygenator is connected to pulmonary artery-left atrium (PA-LA) and blood is circulated without a pump. Though there are many compact centrifugal and axial blood pumps that are commercially available, it is difficult to achieve uniform inflow at the fiber bundle inlet of the oxygenator given that the inlet port has a small diameter, and there is limited space. A high flow speed from the small diameter port causes complex flow in the inlet part of the AIL.[5] This complex flow is the cause of thrombus formation, because the activated procoagulant molecules easily pool in the stagnation area. To avoid this problem, the blood pump for the AIL should be designed to have a wide and uniform outflow. We developed an integrated implantable pump oxygenator using a cross-flow pump (CFP) that can produce a uniform flow to the oxygenator within a limited space.[6–9] The blood flow pattern in an oxygenator depends on the shape of the inlet part.[1] Uniform flow in a fiber bundle is necessary in order to increase the efficiency of the hollow fiber membrane part. If blood flows out from the oxygenator without fully contacting the hollow fiber membrane, gas exchange performance deteriorates; however, if blood stays and does not flow out from the stagnation area when stagnation occurs in the hollow fiber, gas exchange performance deteriorates. Furthermore, if high blood flow causes channeling, and blood flows through a part of the hollow fiber membrane, the contact time and the contact area for O_2 gas are decreased, and gas exchange performance is reduced. Because the membrane's surface area will be used effectively only if the flow velocity in the hollow fiber is uniform, the highest gas exchange performance in the oxygenator is shown under such conditions. To achieve uniform flow, kinetic energy has to be changed efficiently to pressure energy at the inlet part. The CFP can convert kinetic energy to pressure energy efficiently because it has a wide impeller and outlet. In this study, we evaluated the effects on the performance of the oxygenator by examining the uniformity of blood velocity at the hollow fiber membrane part with the CFP.

Materials and Methods

Cross-Flow Pump

The structure of the CFP is shown in Figure 1. The CFP impeller has an inner diameter of 21 mm, an outer diameter of

*Department of Electronic and Computer Engineering, Tokyo Denki University, Japan.; †Frontier R&D Center, Tokyo Denki University, Japan.; ‡Shimane Medical University, Japan.; §Hyogo Prefecture Health Promotion Association, Japan.

Submitted for consideration June 2005; accepted for publication in revised form February 2006.This study was supported by the Tokyo Denki University Frontier Research and Development Center.

Address correspondence: Yuichi Asakawa, Department of Electronic and Computer Engineering, Tokyo Denki University, Ishizaka, Hatoyama Machi, HikiGun, Saitama 350-0394, Japan., Phone:+81-492-96-2911 Ex.3154 Fax:+81-492-96-6413.

DOI: 10.1097/01.mat.0000216165.21432.ee

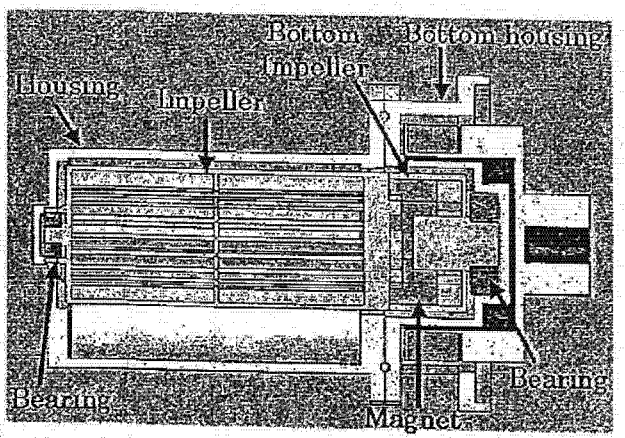

Figure 1. Cross-sectional schematic of the cross-flow pump.

30 mm, and a height of 67.5 mm. The outlet blade angle is set at 30 degrees, and the inlet blade angle is set at 90 degrees. The impeller has 18 vanes.[6–10] The structure of the impeller is shown in **Figure 2**. The CFP has an outlet of 10 mm × 66 mm. Experimental results show that this impeller design has the highest energy efficiency. The impeller was connected to a DC motor through a magnetic coupling. The performance of the CFP was measured during the *in vitro* experiments. The circuit was filled with glycerin having a viscosity of 3.3 cP. The flow rate and pressure head of the CFP were measured at pump speeds of 1400, 1800, 2200, 2600, and 3000 rpm. At each motor revolution speed, the pressure head, determined as the difference between the inflow and outflow pressures, was varied by partial clamping of the outflow tube, and the pump flow rate was measured. The experimental circuit consisted of the reservoir, the CFP, a flow meter TS410 (Transonic Systems Inc., Ithaca, NY), and a pressure meter RM-6000 (Nihon Kohden CO., Tokyo, Japan).

Oxygenator

Based on our hypothesis, the standard deviation of the flow rate was used as the evaluation index that indicated the variation of flow velocity in the fiber bundle. When blood flows uniformly to the fiber bundle, the standard deviation of the flow rate is smaller. The standard deviation of the flow rate in the fiber bundle was calculated using the following formula:

$$\sigma = \sqrt{\frac{1}{n}\sum_{i=1}^{n}\left(x_i - \bar{x}\right)^2}$$

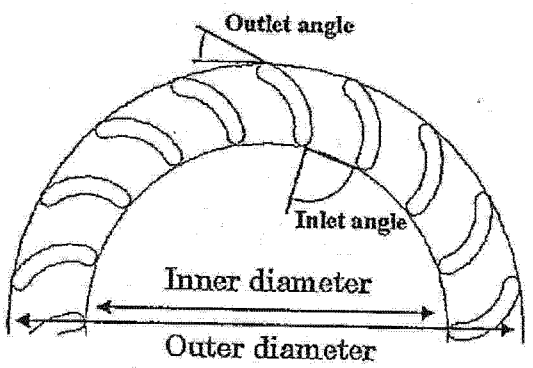

Figure 2. Blade profile for the impeller.

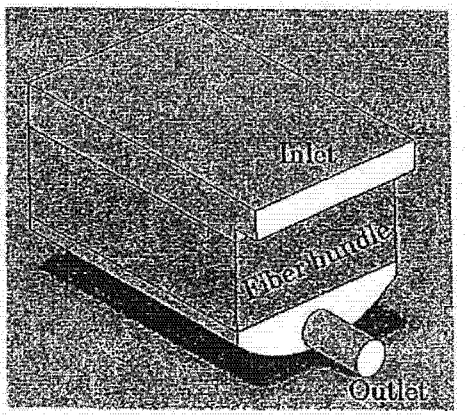

Figure 3. Shown is the standard model that used an improved inlet part of the oxygenator to fit the outlet of the CFP.

where σ is the standard deviation of the flow rate in the fiber bundle, x_i is the flow velocity in each cell, $\bar{x}$ is the average flow velocity of the target cell, and n is the number of cells. The second objective was to minimize the standard deviation of the flow rate in the fiber bundle to obtain better gas exchange performance.[1]

The improved model of αCUBE 6000 (Dainippon Ink & Chemicals Co., Tokyo, Japan) was used as the original design.[1] The oxygenator has a 3/8-inch port. The fiber bundle (DIC membrane) porosity is 0.6, and the membrane surface area is 1.3 m^2. Priming volume is 210 ml. **Figure 3** shows the oxygenator model that uses an improved inlet port to fit the outlet of the CFP. The oxygenator has an inlet port of 10 mm × 66 mm. Each of the three models of the improved oxygenator has a different inlet part. The design parameters set up an inlet taper angle α (**Figure 4**). We selected three representative shapes of the inlet housing that resulted in different α values. Design 1 was the improved standard model. In design 2 α was 10 degrees, while in design 3 α was 40 degrees.

Simulation software, STAR-LT (CD-adapco, Japan), was employed to simulate the flow in the oxygenator. The fluid functioned as a Newtonian fluid. In the current study, the physical properties of blood were assumed to have a viscosity of 3.3×10^{-3} Pa·s and a density of 1060 kg/m^3. The inlet flow rate was 3 l/min. It is difficult to model on a computer the hollow fiber bundle with a complicated structure such as a filter. The hollow fiber bundle part was calculated as a porous medium. The calculation conditions and boundary conditions are shown in **Table 1**.[1,11,12]

In Vitro Experiment

Gas exchange performance was measured in an *in vitro* experiment and was evaluated using the single path method.

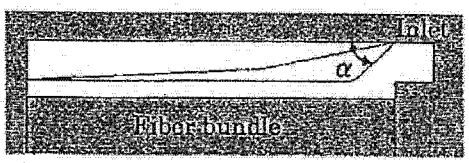

Figure 4. Design variables of the inlet angle. The inlet taper angle α is changed and selected 0 degrees, 10 degrees, 40 degrees.